Estimation of the Persistence of the Effect of a Porous Surface on the Adjacent Turbulent Flow

J. Jiménez, A. Pinelli AND M. Uhlmann
School of Aeronautics, Universidad Politécnica de Madrid

(June 1999)

We perform a direct numerical simulation (case 22) of plane channel flow with two impermeable walls. The initial field is taken from a previous simulation (case 15) in which the lower wall was a no-slip porous surface with the wall-normal transpiration velocity given by Darcy's law:

$$v^+ = -\beta p^+ , \qquad \text{where} \quad v^+ = \frac{v^*}{u_\tau},\ p^+ = \frac{p^{*\prime}}{\rho^* u_\tau^2} \quad . \tag{1}$$

Thus we simulate the relaxation process of the flow as the effect of the former wall porosity decays *temporally*. As a main effect a considerable increase in skin friction (about 30 %) caused by large-scale, spanwise-oriented, roller-like structures had been observed previously [1]. Details of the simulation code are contained in the above reference; the specification of the computational grid and other parameters are given in table 1.

run	L_x/h	L_z/h	N_x	N_y	N_z	Δx^+	Δz^+	Δy^+_{min}	Δy^+_{max}	$\mathrm{Re} = U_0\,h/\nu$	β
case 15	8.17	3.14	256	192	192	9.6	5.0	.20	2.2	3250	0.058
case 22	8.17	3.14	256	192	192	9.6	5.0	.20	2.2	3250	0

Table 1: Parameters of the simulations, concerning the box size, the resolution, outer flow Reynolds number and the Darcy coefficient of porosity. The stream- and spanwise grid spacing corresponds to the number of modes after dealiasing.

Results of the simulation

The time history of the wall friction is plotted in figure 1. The results from the present decay experiment (case 22) are compared to the continuation of the porous/impermeable configuration of case 15. The top wall shear is visibly little affected. On the bottom wall, the value of the friction factor approaches the level of the top wall asymptotically. After an elapsed time of $t\,U_0/h = 3$, the difference in wall friction between the two walls has been reduced to about 5%.

Figure 2 shows spanwise-averaged skin-friction as a function of the streamwise coordinate at different instants during the initial phase of the present simulation (case 22). It can be observed that the initial cyclic (sine-like) shape has disappeared by $t\,U_0/h = 1.6$ giving way to a much smoother streamwise variation.

Figure 3 shows the time variation of the 2d mode ($k_z = 0$, movement in the (x, y)-plane) of the perturbations of streamwise velocity, defined as

$$u'_{2D}(y) = \sqrt{\sum_{k_x} \hat{u}(k_x, k_z = 0, y) \cdot \hat{u}^*(k_x, k_z = 0, y)} \quad , \tag{2}$$

where $\hat{u}(k_x, k_z, y)$ is the Fourier transform of streamwise velocity in streamwise ($x \to k_x$) and spanwise ($z \to k_z$) directions. The figure shows that the decay depends largely on the wall-normal position of the plane under consideration. In the upper half of the channel, the perturbations can be considered as approximately constant. Very close to the bottom wall ($y^+ \approx 5 \ldots 10$) the decay is very rapid (by $t\,U_0/h \approx 3$ the perturbation has decayed to a level similar to that of the flow near the top wall). Only slightly above the viscous sublayer (i.e. for distances $y^+ \geq 17$) the decay is much slower and considerable values of the 2d perturbation persist even at $t\,U_0/h = 8 \ldots 10$.

In figure 4 we have plotted a sequence of instantaneous wall-normal profiles of u'_{2D} spanning the whole time of the simulation. The pronounced peak near the bottom wall is successively smoothed out and shifted towards the interior of the channel. Figure 5 shows that at the same time the wall-normal component v'_{2D} loses much of its initial intensity and the profile approaches a rather symmetric shape. At the latest time, both components are not far from the corresponding profile of the impermeable reference case 16.

Another way of visualizing the decay of the roller-like structures is through isolines of the streamfunction of the 2d perturbations in the (x, y)-plane, Ψ (cf. figure 6). The above sequence of frames allows for a clear distinction of alternating vortex structures until the latest time of the simulation. However, it can be observed that the vortices are progressively restricted to the central part of the channel. The maximum absolute value of the streamfunction decays by about 50% during the simulation.

An important question is the persistence of the change inflicted upon the mean velocity profile by the previous porous wall condition. Figure 8 shows that in the wake region of the profile the return towards a "normal" shape is slow. At the latest time that has been recorded ($t\,U_0/h = 15.1$) a clear deficit between $y/h = 0.8$ and the centerline is still visible. When presented in wall units (cf. figure 9), this deficit appears as a "dent" in the logarithmic region.

Let us consider the results of the experiment in terms of a global shape factor of the channel flow. We calculate the displacement thickness δ^* (cf. figure 10),

$$\delta^* = \int_0^{y(U_{max})} \left(1 - \frac{U}{U_{max}}\right) \mathrm{d}y \quad , \tag{3}$$

and the momentum thickness θ (cf. figure 11),

$$\theta = \int_0^{y(U_{max})} \frac{U}{U_{max}} \left(1 - \frac{U}{U_{max}}\right) \mathrm{d}y \quad , \tag{4}$$

where $U(y, t) = \int_0^{L_x} \int_0^{L_z} u(x, y, z, t) \mathrm{d}z \mathrm{d}x / (L_x L_z)$ and $y(U_{max})$ the wall-normal coordinate of the location where U takes its maximum value. This allows us to follow the evolution of the shape factor $H = \delta^*/\theta$ which is an indicator for the risk of flow separation. Figure 12 shows that the proximity of the porous wall in case 15 has diminished the value of the shape factor by about 5%. During the present experiment, this quantity increases very slowly and has recovered only one third of that difference by the latest elapsed time of 15 outer flow units. This observation implies that the modification of the mean flow has been quite persistent and far-reaching.

Implications for the Lille experiment

Let us assume that a limit for experimental detectability of drag increase is 5%. Then we want to estimate the *distance* behind the porous plate in the Lille experiment that corresponds to the *time* elapsed in our simulation when the drag increase has dropped off to this limiting value.

Outer flow time units $t_o = t\,U_0/h$ are transformed into wall units t^+ by the following equation

$$t^+ = t_0 \cdot \frac{\mathrm{Re}_\tau^2}{\mathrm{Re}}\,, \qquad \mathrm{Re}_\tau = \frac{u_\tau\,h}{\nu} \quad . \tag{5}$$

Since in our simulation the friction Reynolds number Re_τ decreases with time, we use an averaged value: $\mathrm{Re}_\tau = 200$. From figure 1 we see that for $\Delta c_f = 5\%$ the elapsed time is $t_0 \approx 3$, thus $t^+ \approx 37$. In order to convert time elapsed into distance covered, we consider a velocity $U_c^+ = 10$ which corresponds approximately to the phase velocity of most near-wall structures [2] as well as to that of roller-like structures above the porous wall [1]. Therefore: $x^+ = t^+\,U_c^+ = 370$. In Lille dimensions (i.e. viscosity of ambient air and $u_\tau = 0.5\,m/s$) this distance corresponds to $x = 0.011\,m$.

On the other hand, figures 3 and 6 show that the remnants of the spanwise organized structures should be discernible at much larger distances behind the porous boundary element. However, in order to be able to achieve this, the measurement/visualization needs to be performed outside the immediate (viscous-dominated) wall region (say $y^+ \geq 30$).

Conclusion

We have simulated the temporal decay of the effect of porosity on a turbulent flow in a plane channel after the porosity of the wall has been switched off. Our numerical results show that the enhancement of skin friction decays to one sixth of its initial value within 37 viscous time units. This corresponds to about $1\,cm$ in the Lille wind tunnel.

Spanwise-coherent, roller-like structures roughly span the whole channel height. Therefore their part that is situated outside the viscous wall-region persists for much larger times and is believed to be discernible at several multiples of the above mentioned characteristic distance for increased skin friction.

Finally, the shape factor H of the mean streamwise velocity profile is found to return towards its reference value very slowly. After 15 outer flow time units have elapsed, only one third of the initial deficit has been recovered. This fact indicates that wall porosity has a long-lasting effect upon the mean flow.

References

[1] J. Jiménez, A. Pinelli, and M. Uhlmann. Plane channel flow simulation over porous walls. Technical Note ETSIA MF-9809, School of Aeronautics, Universidad Politécnica Madrid, Spain, 1998.

[2] J. Jiménez and P. Moin. The minimal flow unit in near-wall turbulence. *J. Fluid Mech.*, 225:213–240, 1991.

Figures

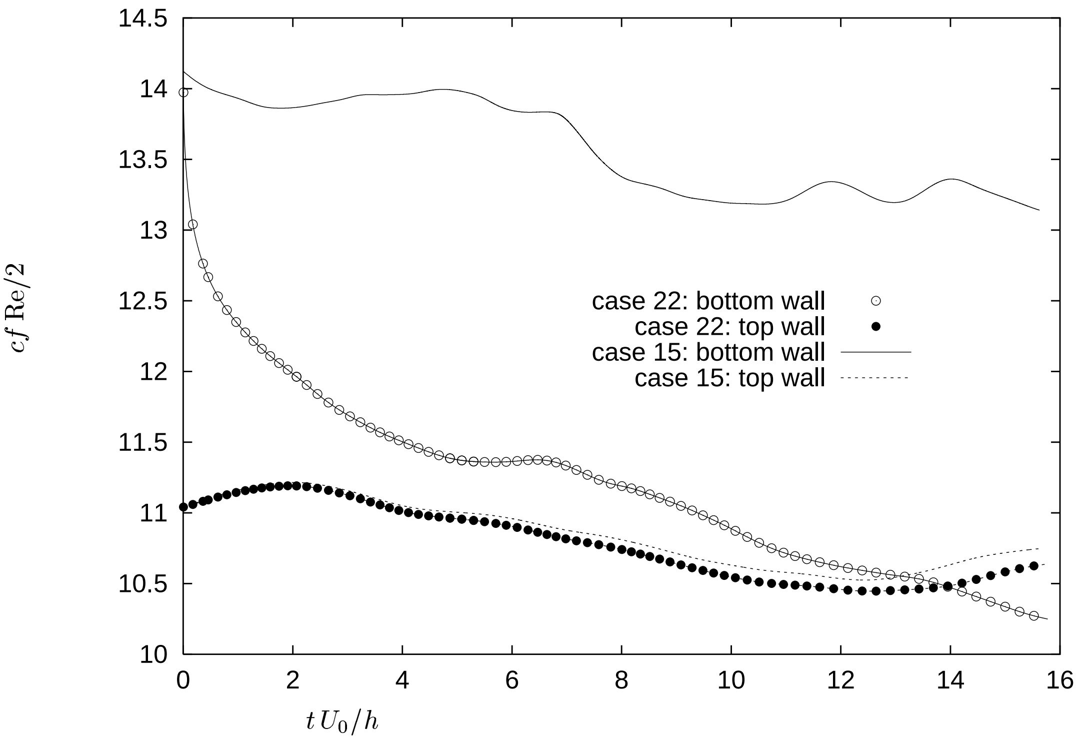

Figure 1: Temporal variation of the friction coefficient averaged over the respective wall plane.

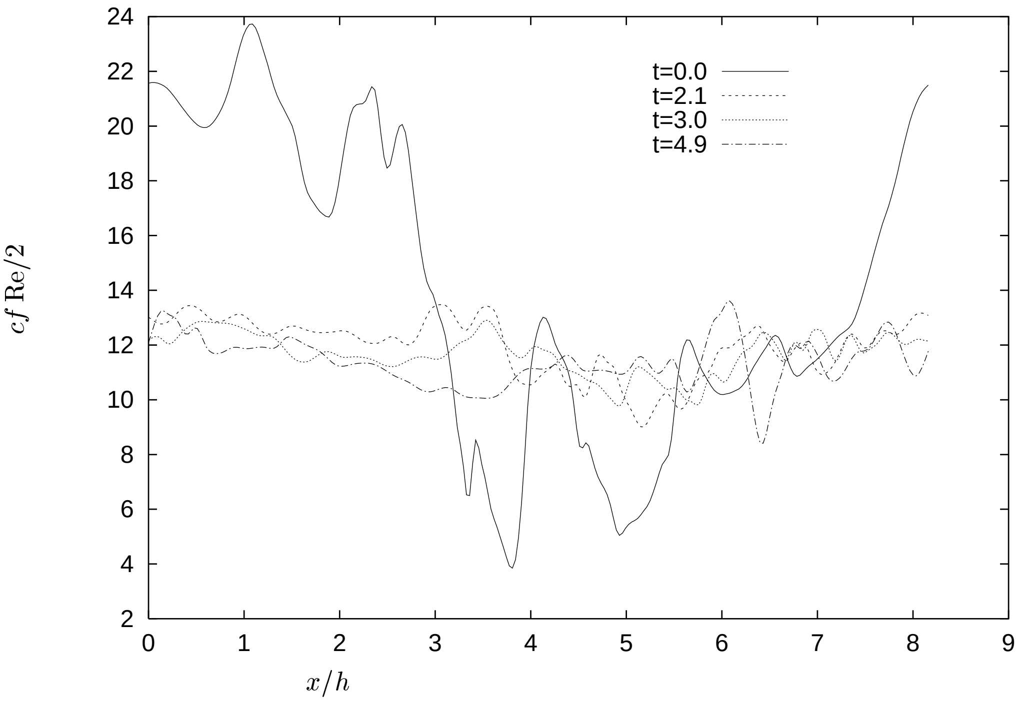

Figure 2: Spanwise averaged skin friction on the bottom wall as a function of streamwise coordinate and taken at different instants of the time series.

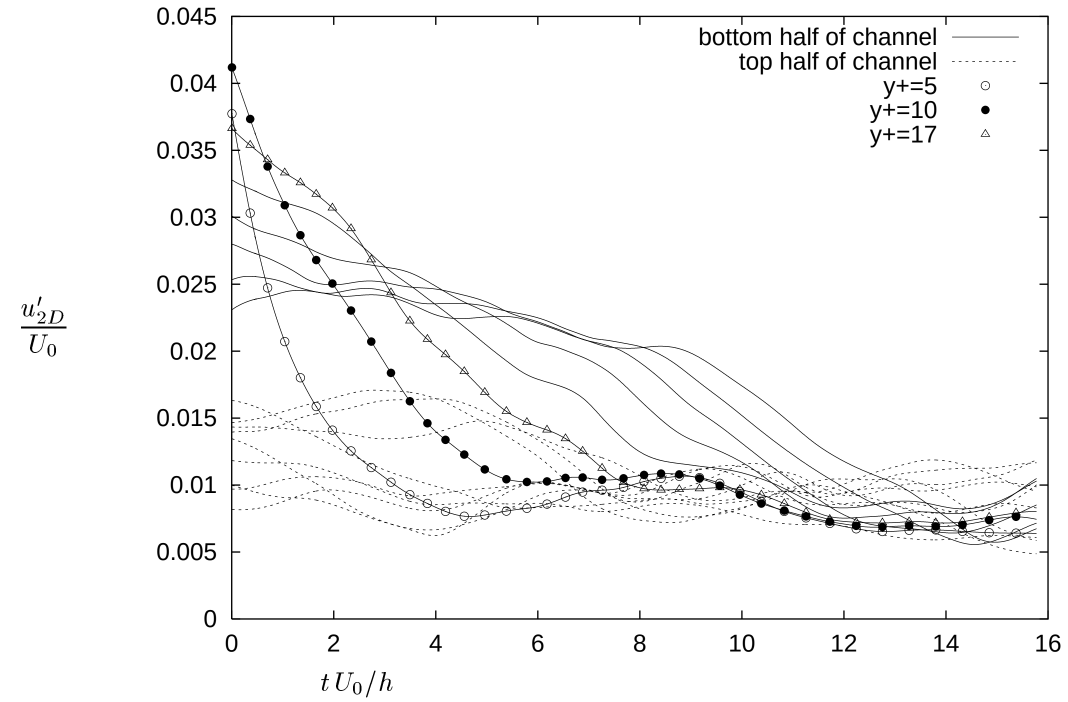

Figure 3: Temporal variation of the perturbations of streamwise velocity which are constant in the spanwise direction (i.e. $k_z = 0$ modes), averaged over respective planes (x, z). The wall-distances near both walls are in the range of $y^+ = 5 \ldots 50$.

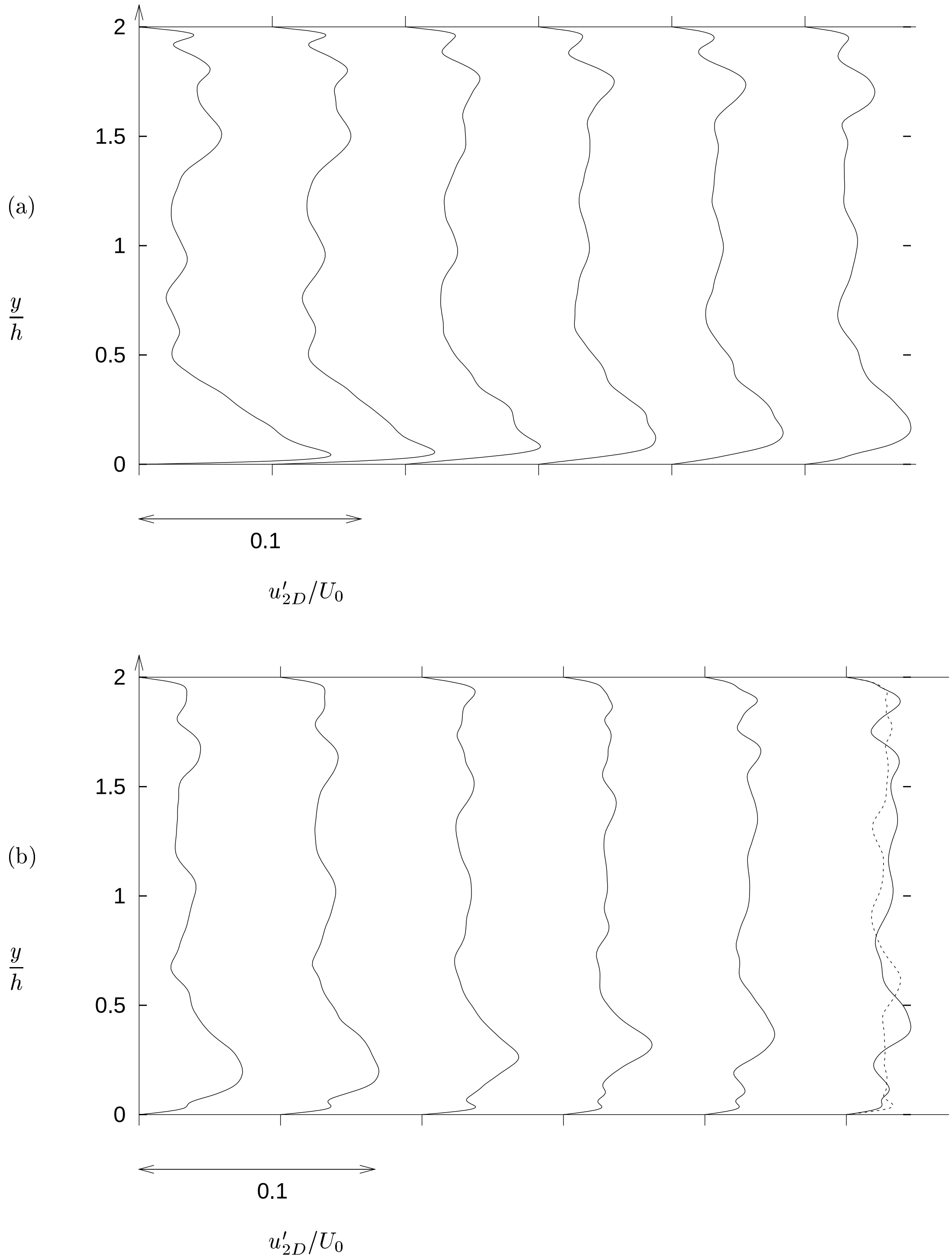

Figure 4: Wall-normal profiles of the perturbations of streamwise velocity which are constant in the spanwise direction (i.e. $k_z = 0$ modes), averaged over respective planes (x, z). Successive profiles represent a time series at times: (a) $tU_0/h = \{0.0, 0.5, 2.1, 3.0, 4.0, 4.9, 6.4\}$, (b) $tU_0/h = \{7.3, 9.2, 11.3, 13.8, 15.1\}$. The ticmarks on the abscissa indicate the origin of the respective profiles. The dashed line overlayed upon the last profile in the series (b) corresponds to an instantaneous profile of the reference case 16 (impermeable).

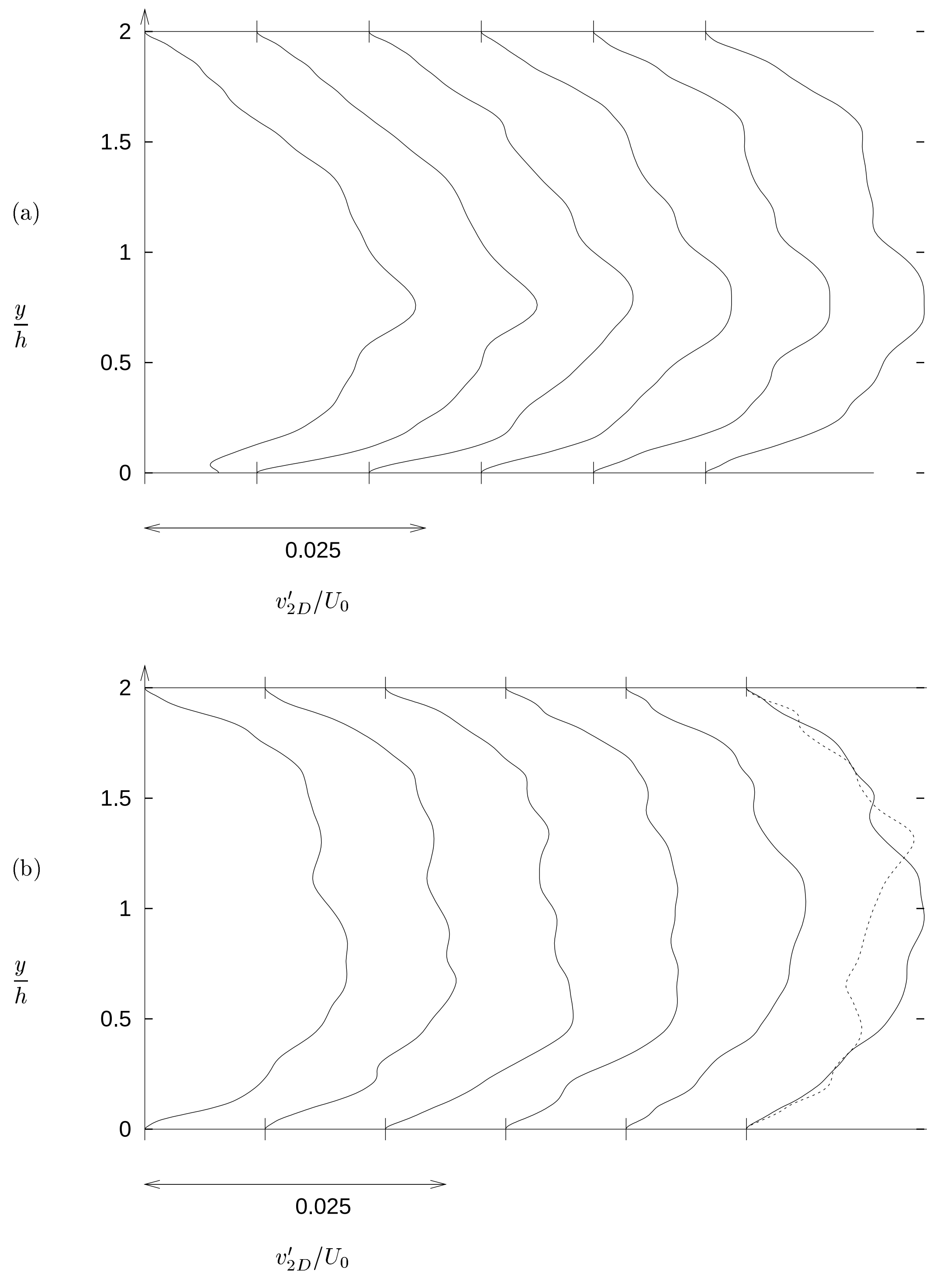

Figure 5: Wall-normal profiles of the perturbations of wall-normal velocity which are constant in the spanwise direction (i.e. $k_z = 0$ modes), averaged over respective planes (x, z). Successive profiles represent a time series at times: (a) $t\,U_0/h = \{0.0, 0.5, 2.1, 3.0, 4.0, 4.9, 6.4\}$, (b) $t\,U_0/h = \{7.3, 9.2, 11.3, 13.8, 15.1\}$. The ticmarks on the abscissa indicate the origin of the respective profiles. The dashed line overlayed upon the last profile in the series (b) corresponds to an instantaneous profile of the reference case 16 (impermeable).

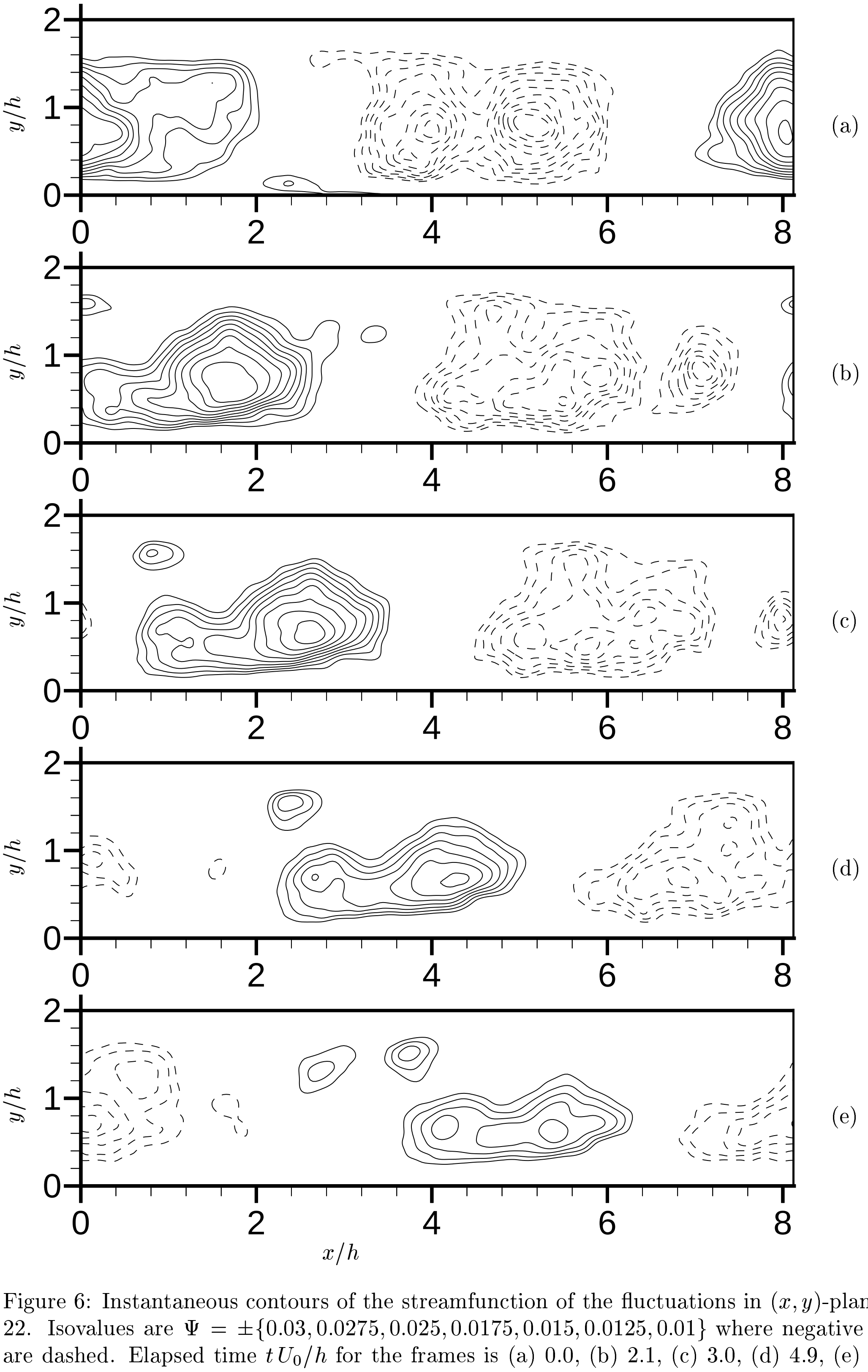

Figure 6: Instantaneous contours of the streamfunction of the fluctuations in (x, y)-plane of case 22. Isovalues are $\Psi = \pm\{0.03, 0.0275, 0.025, 0.0175, 0.015, 0.0125, 0.01\}$ where negative contours are dashed. Elapsed time tU_0/h for the frames is (a) 0.0, (b) 2.1, (c) 3.0, (d) 4.9, (e) 6.4. The mean flow is in positive x-direction. The maximum absolute value has decayed from 0.033 to 0.021 between frames (a) and (e).

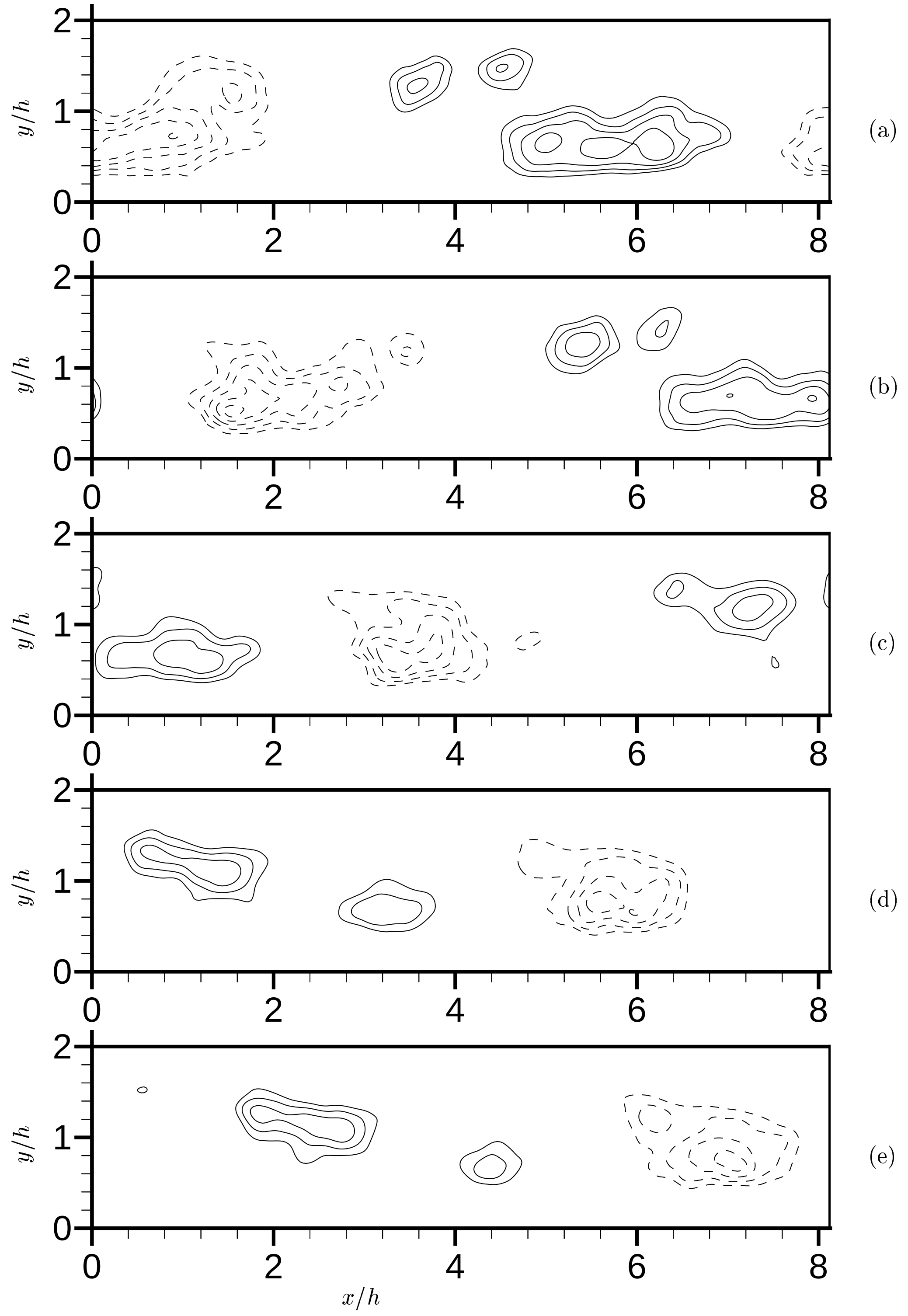

Figure 7: Instantaneous contours of the streamfunction of the fluctuations in (x, y)-plane of case 22. Isovalues are $\Psi = \pm\{0.03, 0.0275, 0.025, 0.0175, 0.015, 0.0125, 0.01\}$ where negative contours are dashed. Elapsed time tU_0/h for the frames is (a) 7.3, (b) 9.2, (c) 11.3, (d) 13.8, (e) 15.1. The mean flow is in positive x-direction. The maximum absolute value has decayed from 0.020 to 0.018 between frames (a) and (e).

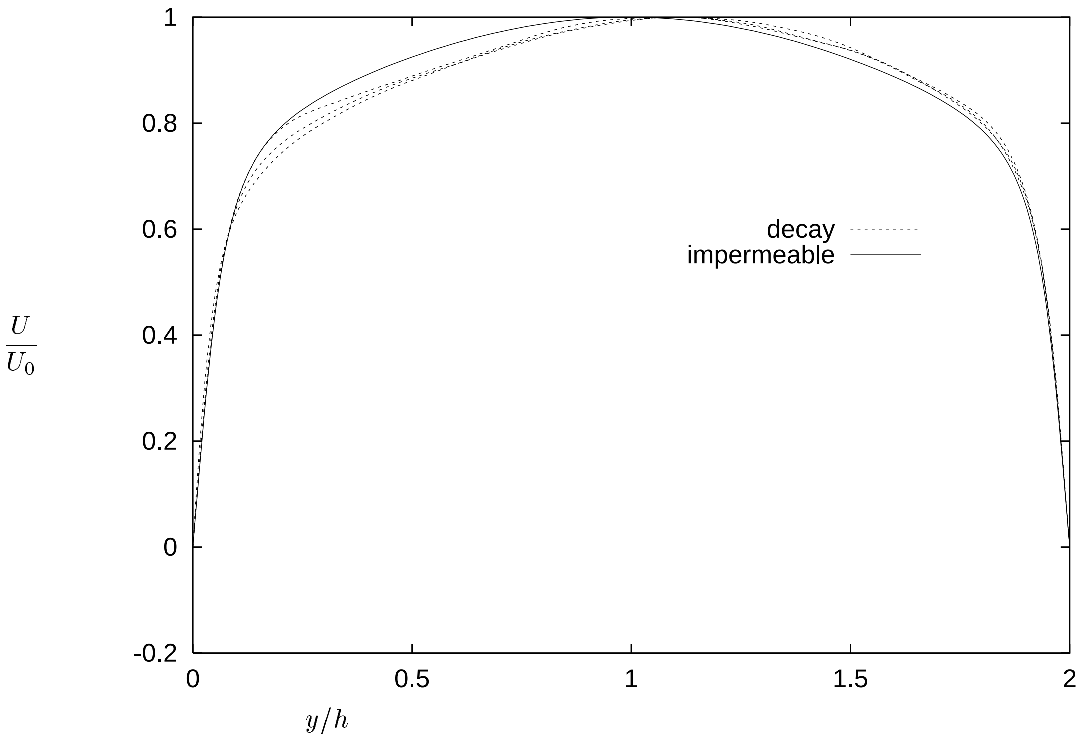

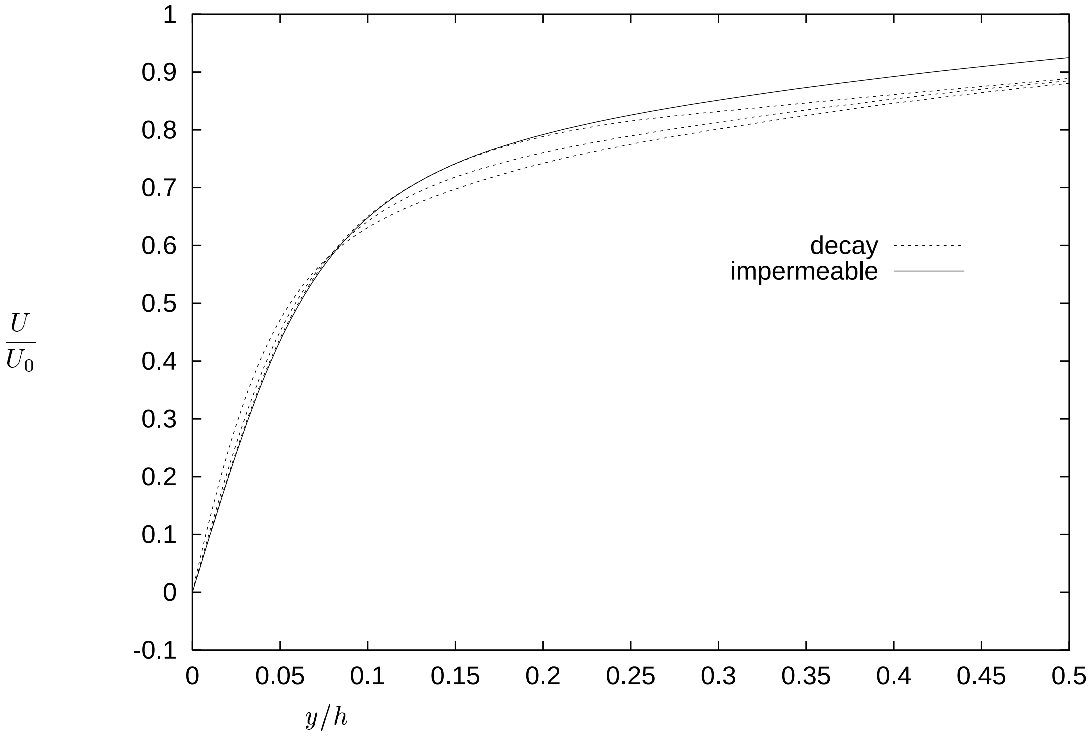

Figure 8: Wall-normal profiles of the box-averaged instantaneous streamwise velocity U at different times of the present simulation $t\,U_0/h = \{0.0, 9.2, 15.1\}$. The box-averaged and time-averaged data of the reference case 16 (impermeable) is also given.

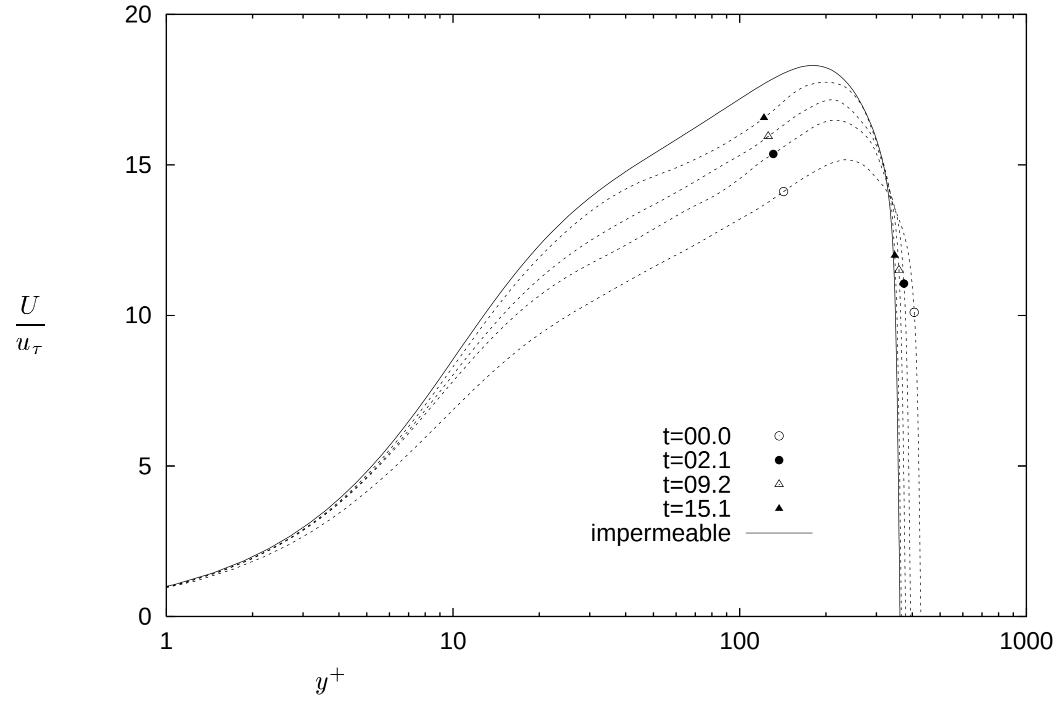

Figure 9: Wall-normal profiles of the box-averaged instantaneous streamwise velocity U at different times of the present simulation $t\,U_0/h = \{0.0, 9.2, 15.1\}$, given in wall-units and as a log-lin plot. The box-averaged and time-averaged data of the reference case 16 (impermeable) is also given.

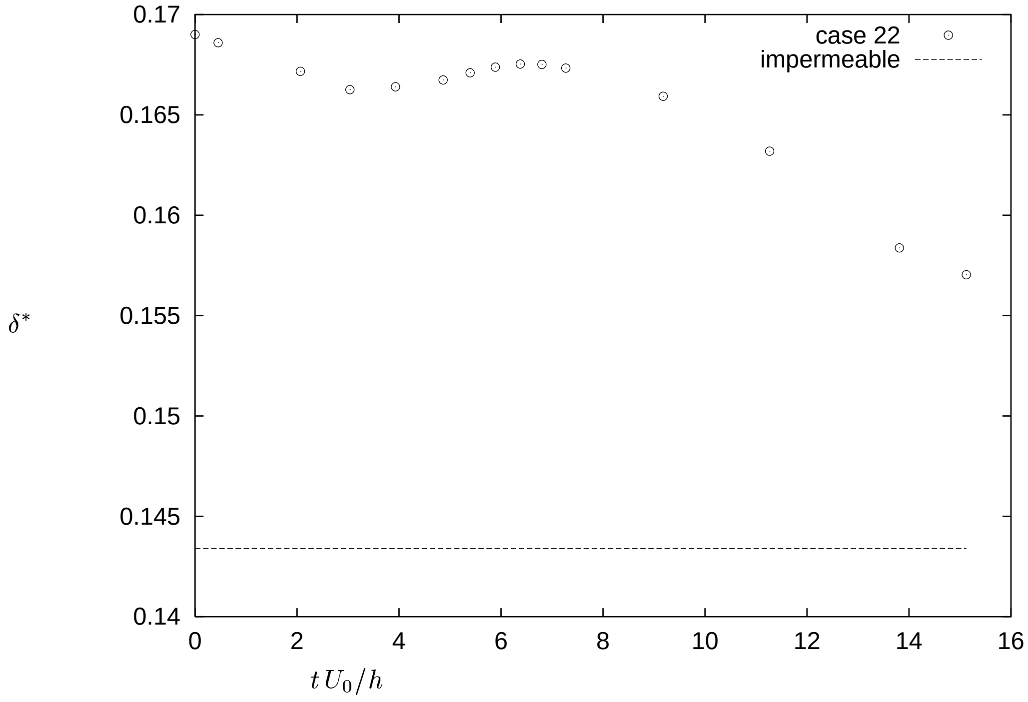

Figure 10: Time variation of the displacement thickness δ^*. The solid line gives the average value of the reference case 16 (impermeable).

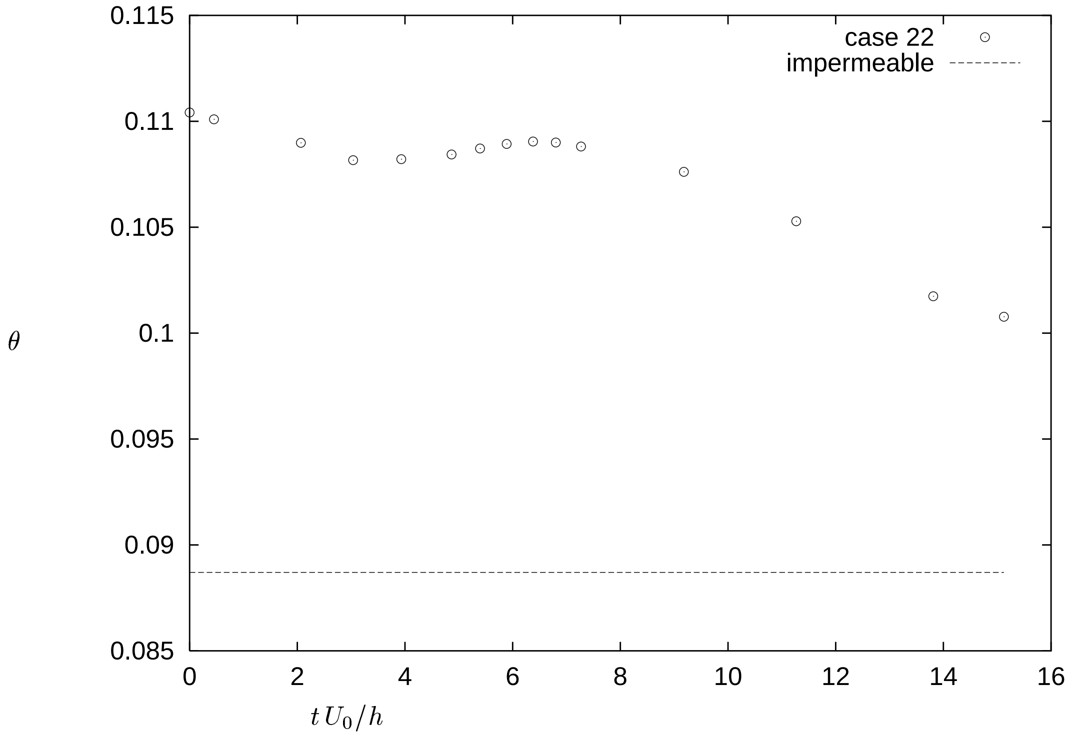

Figure 11: Time variation of the momentum thickness θ. The solid line gives the average value of the reference case 16 (impermeable).

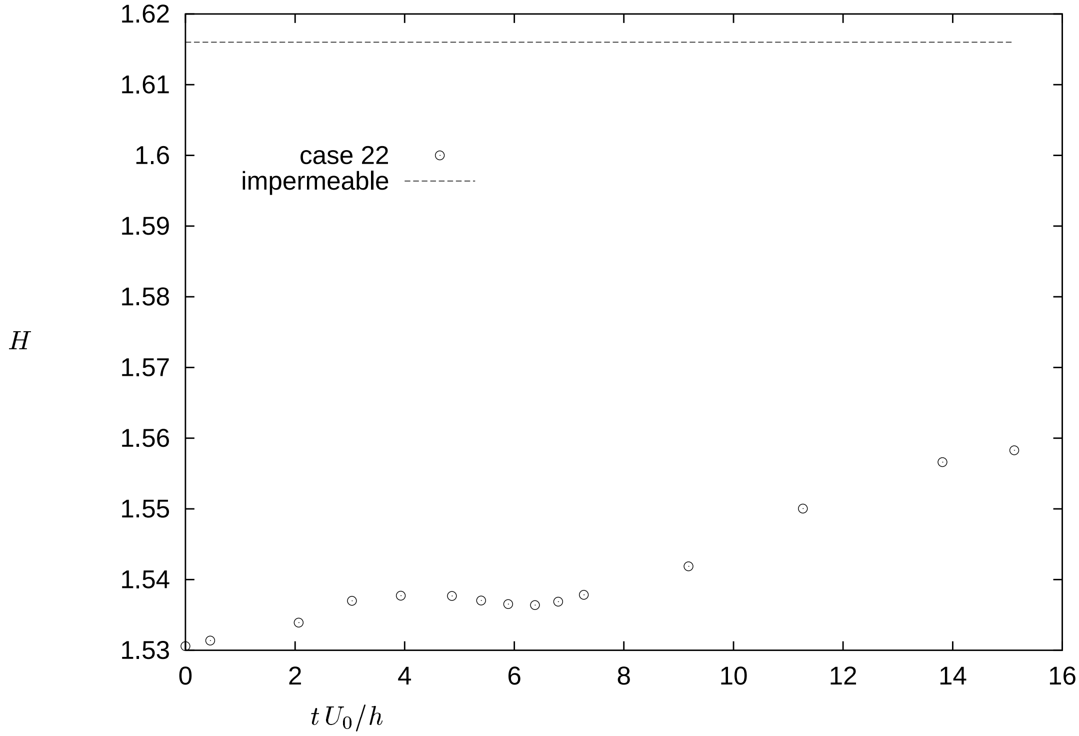

Figure 12: Time variation of the shape factor $H = \delta^*/\theta$. The solid line gives the average value of the reference case 16 (impermeable).